How to cite: Angew. Chem. Int. Ed. 2024, e202418938
doi.org/10.1002/anie.202418938

Chirality Transfer

Biofuel-Driven Stepping Chiral Supramolecular Transfer Container

*Jie Yu[+], Huijia Yu[+], Yugui Qiu, Heng-Yi Zhang, Xiufang Xu, and Yu Liu**

Abstract: Herein, we reported a biofuel-driven recyclable chiral supramolecular transfer container based on hexacationic triphenylamine cage and nucleotides. Possessing rotatable paddle rigid backbones, the artificial receptor effectively encapsulated nucleotides with a high binding constant up to $5.37\times10^5\ M^{-1}$ in water, displaying guest-induced efficient fluorescence enhancement with quantum yield increased from 6.5 % to 16.6 %. Especially, the achiral cage could effectively bind with adenosine triphosphate to activate chirality transfer from substrates to the single molecular container, giving circularly polarized luminescence at 575 nm and positive Cotton effect peaks with significant asymmetric factor ($g_{abs}=+6.4\times10^{-4}$). Meanwhile, the adaptive chiral supramolecule not only has reversible thermal responsiveness but also could stepwise regulate chirality transfer by the catalysis of hexokinase and apyrase in tandem, showing recovery adaptive chirality after refueled, achieving dynamically regulated programmable multistate chiral luminescent supramolecules. Therefore, the biofuel-driven chiral supramolecular transfer container could be successfully applied in chiral logic gates and multilevel information encryption, providing new insight into intelligent chiral materials.

Chiral supramolecular materials responsive to external stimuli, such as light, redox, pH, solvent, and enzyme[1–12] have become an important research topic because of their broad applications in chiroptical switches,[13–15] catalysis,[16–17] sensing,[18–20] and information encryption.[21–22] Among them, chiral supramolecules based on macrocycles can integrate chiral units, responsive motifs, and luminescent groups by the hydrophobic, electrostatic, and hydrogen bond interactions between host and guest.[23–26] This is conducive to the directional chirality transfer and amplification and can also realize the precise regulation of chiroptical performance, thereby achieving the functionalization of chiral assemblies. Many pioneering and excellent works involving molecular machines,[27–28] host–guest complexes,[29–30] and multi-dimensional assemblies[31–33] were devoted to the exploration of intelligent chiral supramolecular materials. For example, Lee and co-workers[34] reported that the chirality of pillar-[5]thiacrown was inversed by the coordination of Hg^{2+} and recovered in the presence of S^{2-} or I^- to remove complex cationic. Stoddart et al. found that 1-pyrene carboxylic acid was encapsulated by γ-cyclodextrin at a 2:1 stoichiometric ratio in the cyclodextrin-based metal–organic framework (MOF) and confined by the helix-like chiral superstructure of the MOF to give circularly polarized luminescence (CPL) with high asymmetric factor ($g_{lum}=+3.5\times10^{-3}$) and quantum yield (QY) up to 38 %.[35] Yang group[36] demonstrated that the anion could modulate the movement of the chiral wheel in [3]rotaxanes, then regulate aggregation behaviors and affect the chiral luminescence performance. Liu group reported a series of chiral supramolecular assemblies.[37–38] Typically, layered two-dimensional chiral supramolecular polymers based on covalently linked β-cyclodextrin-confined luminophores and triformylphloroglucinol derivatives, which exhibited a high quantum yield of 23.06 % and tunable g_{lum} values by regulating the ratio of macrocycles.[39] Besides the macrocycles mentioned above, multi-charged artificial receptors could also bind nucleotides to form chiral supramolecules by chirality transfer from chiral guests to achiral hosts. Compared with acyclic,[40–42] macrocyclic,[43–45] and bicyclic hosts,[46–47] multi-charged artificial macrocycles have unique advantages in forming tunable chiral supramolecular assemblies by multivalent interactions. For example, the Cao group[48] found that the achiral cationic anthracene macrocycle could effectively encapsulate biomolecule-adenosine triphosphate (ATP) to give induced *M*-twisted conformation adaptive chiral complex, which further boosted the formation of intermolecular *P*-twisted anthracene excimer endowing the second-level supramolecular chirality.

It can be seen from the above-reported research that intelligent chiral supramolecular assemblies were not only constructed by the chiral host-induced achiral guest but also achieved by the assembly of the chiral guest-activated achiral host, displaying various stimulus responsiveness chiral supramolecular functions. However, using biomolecular guests as biofuel to induce achiral host achieving chiral supramolecular assembly, and then directionally step-by-step regulate chiral transfer by consuming biomolecules under the enzymes catalysis is rarely reported. In this work, we wish to report that the hexacationic tricyclic triphenylamine cage could effectively encapsulate guest-ATP to enhance host fluorescence by strong binding affinity and form the reversible thermal responsiveness adaptive chiral supramolecule. Furthermore, the biomolecular ATP could act as biofuel in chiral supramolecular containers to achieve stepping-regulated chirality transfer by the catalysis of enzymes in tandem (Scheme 1), which could be successfully applied in chiral logic gates and information encryption.

[*] J. Yu,[+] H. Yu,[+] Y. Qiu, H.-Y. Zhang, X. Xu, Prof. Y. Liu
College of Chemistry, State Key Laboratory of Elemento-Organic Chemistry, Nankai University
Tianjin 300071 (P. R. China)
E-mail: yuliu@nankai.edu.cn

[+] These authors contributed equally to this work.

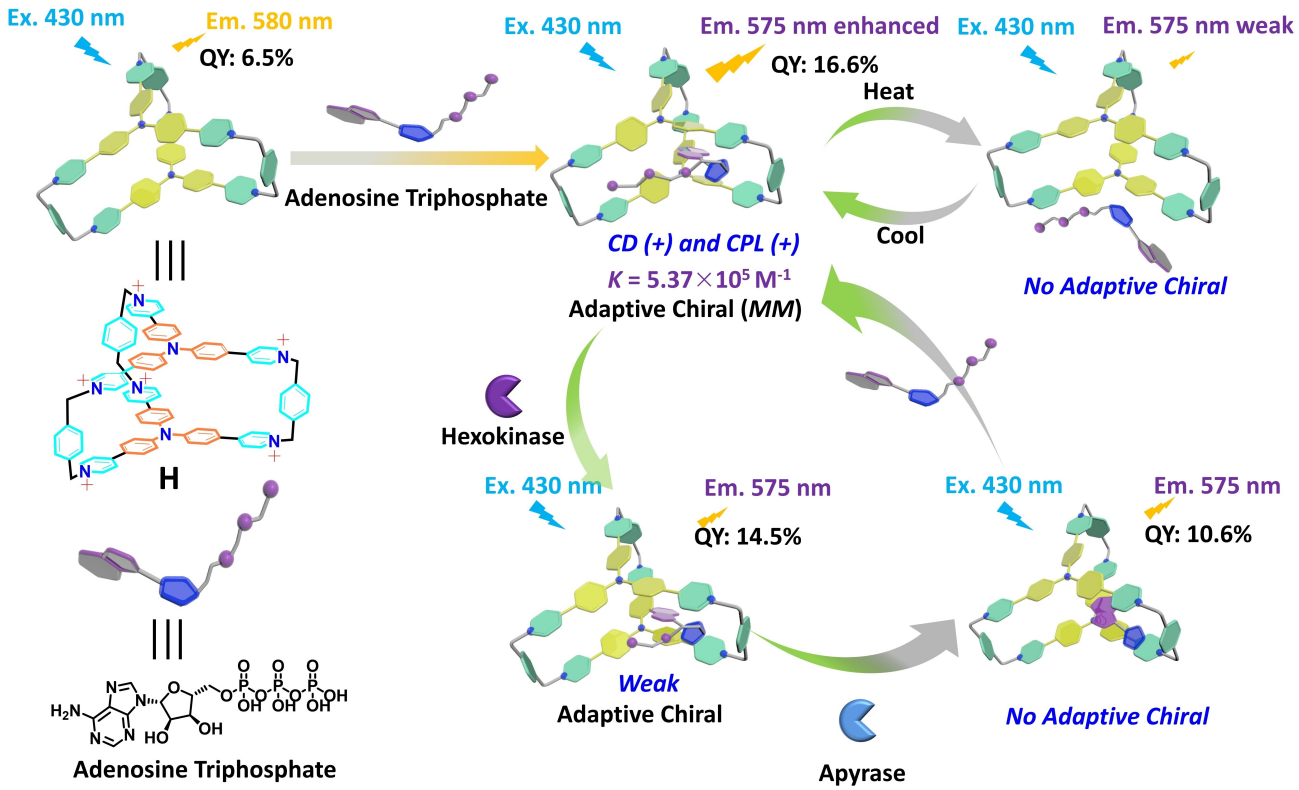

Scheme 1. Biofuel-driven stepping chiral supramolecular transfer container.

Hexacationic cage was synthesized by the two-step S_N2 reaction. Concretely, compound 1 reacted with excess 1,4-bis(bromomethyl)benzene to give tricationic compound 2, then further reacted with 1 and exchanged anions to obtain water-soluble artificial receptor H as a yellow solid (Scheme S1). The structure of the cage was confirmed by nuclear magnetic resonance (NMR) and high-resolution mass spectrometry (Figures S1–S5). The hexacationic H with electron-rich triphenylamine cores and electron-withdrawing pyridinium units may exhibit good photophysical properties. Compared with acyclic TPA (Scheme S1), the absorption peak of H appeared at 430 nm, giving a 5 nm hypsochromic shift (Figure 1a), and the fluorescence signal of H was blue-shifted to 580 nm. The QY of H was also higher than TPA, enhancing from 1.6 % to 6.5 % (Figure S6), indicating the covalent connected three methylene phenyl bridges of the cage decreased or limited the vibration and rotation of triphenylamine units, then beneficial to the luminescence. The receptor H exhibits good luminescent performance in water and has rigid triphenylamine cores and a precise confinement cage cavity, which is suitable for recognizing substrates. Subsequently, the binding behavior of H to nucleotides was investigated by the UV/Vis titration experiments. In Figure 1b, the ATP induced the characteristics absorption peak of H red-shifted from 430 nm to 450 nm. According to the change of absorption peak at 450 nm (Figure S7), the apparent binding constant between H and ATP was measured as $5.37\times10^5\ M^{-1}$ using a 1:1 binding ratio.[49] After adding adenosine diphosphate (ADP), adenosine monophosphate (AMP), and adenosine (AD), the absorption signal of H also red-shifted to 448 nm, 440 nm, and 434 nm (Figures 1c–d and S8), respectively, giving weaker binding affinity (Figure S9). Compared with H/ATP, the binding constant between AMP and H decreased 5.2-fold because AMP has fewer phosphate units and thus could not provide sufficient electrostatic interaction sites as ATP.

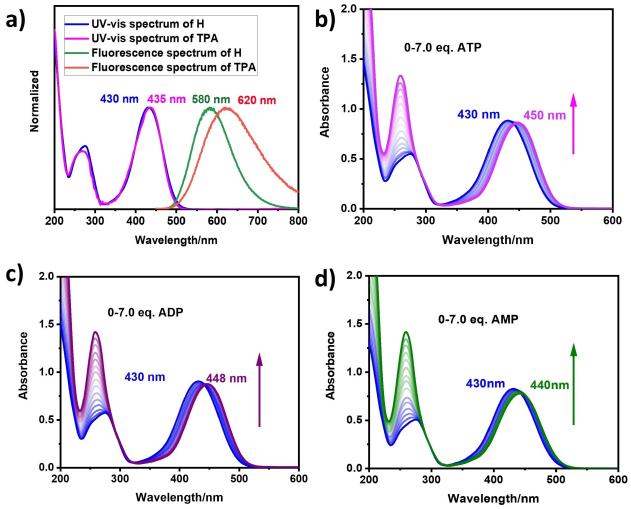

Figure 1. (a) Normalized UV/Vis and fluorescence spectra of H and TPA at 25 °C. UV/Vis spectra of H with the addition of (b) ATP (c) ADP, and (d) AMP at 25 °C ([H] = [TPA] = 0.01 mM).

Especially, adenosine without anion group gave a weak binding constant (Figure S9c, $5.03\times10^{3}\ M^{-1}$) to the cage, decreasing 106-fold compared with H/ATP, manifesting the cationic cage possesses excellent selective recognition ability. In addition, the other nucleotides, including guanosine triphosphate (GTP), cytidine triphosphate (CTP), and uridine triphosphate (UTP) (Figure S9d), could also lead to the absorption peak of H red-shifted to 450 nm, 440 nm, and 442 nm, and the binding constants were calculated as $1.22\times10^{5}\ M^{-1}$, $1.26\times10^{5}\ M^{-1}$, and $1.10\times10^{5}\ M^{-1}$, respectively (Figures S10–12), showing strong binding capability of the receptor to nucleotides.

Subsequently, NMR and isothermal titration calorimetry (ITC) experiments were performed to investigate the binding behaviors of the cage to nucleotides. The protons of H were reasonably ascribed by the 2D NMR spectrum of hexacationic cage in water (Figure S13). Figure 2a showed that the protons of $H_{1,2}$ in ATP were upshifted as 1.55 ppm and 1.30 ppm, respectively, and $H_{3,4,5}$ also gave upfield shift (Figure S14), indicating the triphenylamine cage encapsulated the adenine and ribose units of ATP. Meanwhile, the protons of $H_{e,f}$ in the cage were upfield shifted from 7.73 ppm and 7.22 ppm to 7.62 ppm and 6.98 ppm, respectively, showing the shielding effect for the protons of triphenylamine core derived from the π–π and hydrophobic interactions between the adenine group of ATP and triphenylamine. The protons of H_a and H_c were downshifted as 0.06 ppm and 0.03 ppm, which should be attributed to the hydrogen bond interaction between the phosphate and hydroxyl (ribose) groups of ATP and the protons of the pyridinium (H_c) and bridged benzene (H_a). The correlation signals of $H_{1,2}$ and H_f were found in the 2D NOESY spectrum, further confirming the adenine part of ATP was close to the triphenylamine core (Figure S15). The inflection point of the Job plot was 0.5, indicating that the stoichiometric ratio of H/ATP was 1:1 (Figure S16). In addition, the binding model of H/ATP was also confirmed by geometry optimization with the Gaussian 16 program (Figure S17). The ITC experiments showed that the triphenylamine cage binds with ATP gave thermodynamic parameters (Figure 2b) of ΔG, ΔH, and TΔS as $-(7.53)$, $-(10.38\pm0.70)$, and $-(2.85)$ kcal mol^{-1}, respectively, manifesting the binding process was driven by enthalpy deriving from electronic complementarity and multi-noncovalent interaction, including electrostatic, π–π, hydrogen bond, and hydrophobic interactions between receptor and ATP to overcome entropic penalty.[50] The binding constant of H to ATP measured by ITC experiments ($3.34\times10^{5}\ M^{-1}$) was also consistent with the value ($5.37\times10^{5}\ M^{-1}$) tested by UV/Vis titration experiments. For ADP and AMP, the cage gave weaker binding affinities ($1.72\times10^{5}\ M^{-1}$, $1.34\times10^{5}\ M^{-1}$) than ATP (Figures S18–19). The artificial receptor also exhibited weaker binding constants to the other triphosphate nucleotides (GTP, CTP, and UTP) than ATP (Figures S20–22). Therefore, taking advantage of multiple noncovalent interactions, the artificial receptor could effectively bind with nucleotides.

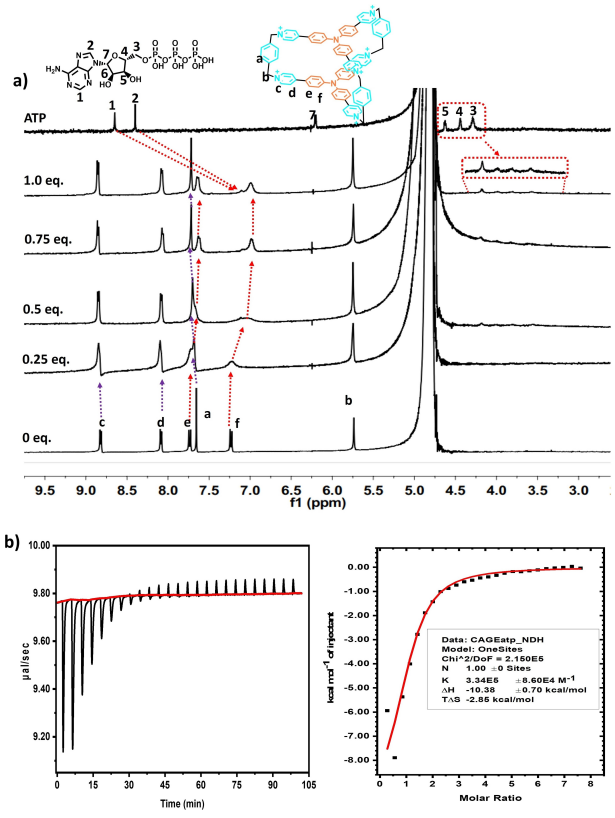

Figure 2. (a) ^{1}H NMR spectra of H (0.4 mM) with the addition of ATP (0–1.0 eq.) in D_2O at 25 °C. (b) ITC profiles for the titration of H (0.01 mM) with ATP at 25 °C.

The hexacationic artificial receptor, with the rigid and rotatable triphenylamine cores, could selectively encapsulate nucleotides with a chiral ribose unit, attracting us to explore chirality transfer between the cage and substrates. As shown in Figure 3a, the positive CD peak at 465 nm was increased and reached the balance after 5.0 eq. ATP was added (Figure 3b). The emerged CD signal at 300–600 nm was corresponding to the UV/Vis signal of H, indicating the chirality of the substrate with the ribose group was transferred to the host, leading to *M* rotational chiral conformation,[51–52] and the asymmetric factor of circular dichroism (g_{abs}) was calculated as $+6.4\times10^{-4}$ (Figure S23). ADP (Figures 3c–d) could also induce the achiral host to give weak CD signals. However, negligible CD signals were observed at 300–600 nm in H/AMP and H/AD (Figure S24), indicating the chirality of AMP and AD could not effectively transfer to the host and further confirming that the strong host–guest interaction was critical to achieving chiral transfer. Compared with ATP, the other three kinds of triphosphate adenosines (GTP, UTP, and CTP) can only induce H to give weaker CD peaks (Figure S25). The g_{abs} of the H induced by GTP, UTP, and CTP were calculated as $+1.1\times10^{-4}$, $+2.3\times10^{-4}$, and $+5.2\times10^{-5}$ (Figure S23), respectively. These results jointly indicated that the supramolecular transfer container's chiroptical properties could be regulated by binding affinities, exhibiting selective chiroptical response to nucleotides. Furthermore, no Cotton effect peak appeared in TPA/ATP at 300–600 nm (Fig-

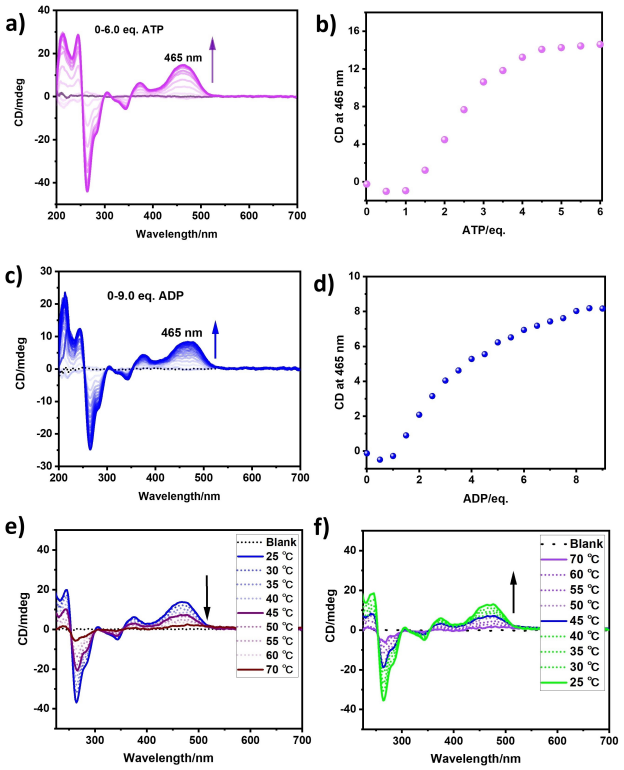

Figure 3. (a) CD spectra of H with the addition of ATP at 25 °C ([H] = 0.01 mM). (b) The change of CD intensity of H at 465 nm in the presence of ATP. (c) CD spectra of H with the addition of ADP at 25 °C ([H] = 0.01 mM). (d) The change of CD intensity of H at 465 nm in the presence of ADP. CD spectra of H/ATP (5.0 eq.) under (e) heating and (f) cooling conditions ([H] = 0.01 mM).

ure S26), indicating the confined cage structure is indispensable for the chiral transfer from substrates to the host.

The hexacationic cage, with a three-dimensional cavity and the π-conjugated aromatic core, encapsulates ATP to form a chirality transfer supramolecular container, which can be dynamically modulated by thermal and enzyme. As can be seen from Figure 3e, the induced peak of H/ATP at 465 nm gradually decreased with the temperature increasing from 25 to 70 °C, indicating the chiral transfer from ATP to the cage was interrupted, which ascribed to the decomplexation of the chiral supramolecules under thermal stimulation. However, the adaptive chiral signal was observed again as the system cooled (Figure 3f); thus, the adaptive chirality supramolecule based on the noncovalent interactions exhibited thermal-reversible response performance. Subsequently, we investigated enzyme-responsive chiral supramolecules using ATP as biofuel and apyrase (AP) as the catalyst. As shown in Figure 4a, the supramolecule's CD signal gradually diminished in the presence of AP, implying that the ATP was consumed under the hydrolysis of AP[53] to yield AD and phosphate (Pi) (Figure S27a–c), resulting in the supramolecule losing adaptive chirality (the red arrow). Subsequent addition of ATP (8.0 eq.), the CD signal was reinduced at 465 nm (the purple arrow), showing the refueling capability of the chiral supramolecule (Figure 4b).

Interestingly, the tandem catalysis of hexokinase (HK) and AP could stepwise regulate the adaptive chirality transfer to achieve programmable regulating multistate chiral supramolecules. Under the catalysis of HK (Figure 4c), the phosphate group of ATP was transferred to glucose (Glu.) to give ADP and glucose-6-phosphate (Glu-6p) (Figure S27d). Thus, the CD intensity of the chiral supramolecule at 465 nm was gradually decreased and reached balance after 20 min (Figure 28a), implying that the chiral transfer was weakened and forming the weaker adaptive chiral supramolecule. After adding AP (Figure 4d), the system's CD signal was further reduced to disappear (the wine arrow), ascribing to ADP was hydrolyzed by AP to yield AD and Pi (Figure S27e), resulting in no adaptive chiral H/AD after 70 min (Figure S28b). Then, the CD signal reappeared at 465 nm (the pink arrow) after ATP (16.0 eq.) was added (Figure 4d), realizing recyclable stepping chiral transfer by the catalysis of HK and AP in tandem (Figure 4e). As a biofuel, the stepping decomposition reaction rates of ATP were $5.96\times10^{-4}\ s^{-1}$ and $4.09\times10^{-4}\ s^{-1}$, respectively (Figures S28cd). This unique adaptive chiral supramolecular transfer container with thermal and enzyme responsiveness achieved the programmable stepping regulation of multistate chiral supramolecules.

In order to investigate the chiroptical performance of supramolecular transfer containers by dynamic regulation, the fluorescence and CPL experiments were performed for cage encapsulating the nucleotides in water. As shown in Figure 5a, the fluorescence signal of H was shifted from 580 nm to 575 nm and enhanced up to 9.8-fold in the presence of ATP (Figure 5b). Compared with ATP, ADP, AMP, and AD could only improve (Figures S29a–c) the fluorescence intensity of H by 3.3, 2.6, and 2.1 times, respectively, since the weaker binding affinities between these substrates and H could not effectively induce fluorescence enhancement of receptor. The cage also showed the fluorescence improvement effect for the other three kinds of nucleosides with triphosphate units (GTP, UTP, and CTP) (Figure S29d–f) but only increased 4.5, 2.4, and 2.1 times (Figure 5b), respectively. Compared with the other nucleosides, ATP induced H to give a higher QY of 16.6 % (Figure S30), further confirming the supramolecular container's highly selective fluorescence sensing ability to substrates. In addition, the fluorescence intensity of TPA slightly increased after ATP was added (Figure S31), indicating the confined cage structure was essential for guest-inducing efficient fluorescence enhancement of the host. Subsequently, we further explored the influence of thermal stimulation and enzyme catalysis on the supramolecular container's chiral luminescence performance. In Figure 5c, the fluorescence of H/ATP gradually decreased with the temperature increasing and giving 50.3 % quenching efficiency. After the system cooled, the fluorescence intensity recovered (Figure 5d). Hence, the fluorescence of H/ATP exhibited thermal-reversible response performance. On the other hand, the fluorescence of H/ATP decreased by 44.9 % (Figure S32) and gave a low QY of 14.5 % in the presence of the HK (Figure S33). After tandem AP catalysis, the fluorescence intensity and QY of the system were further

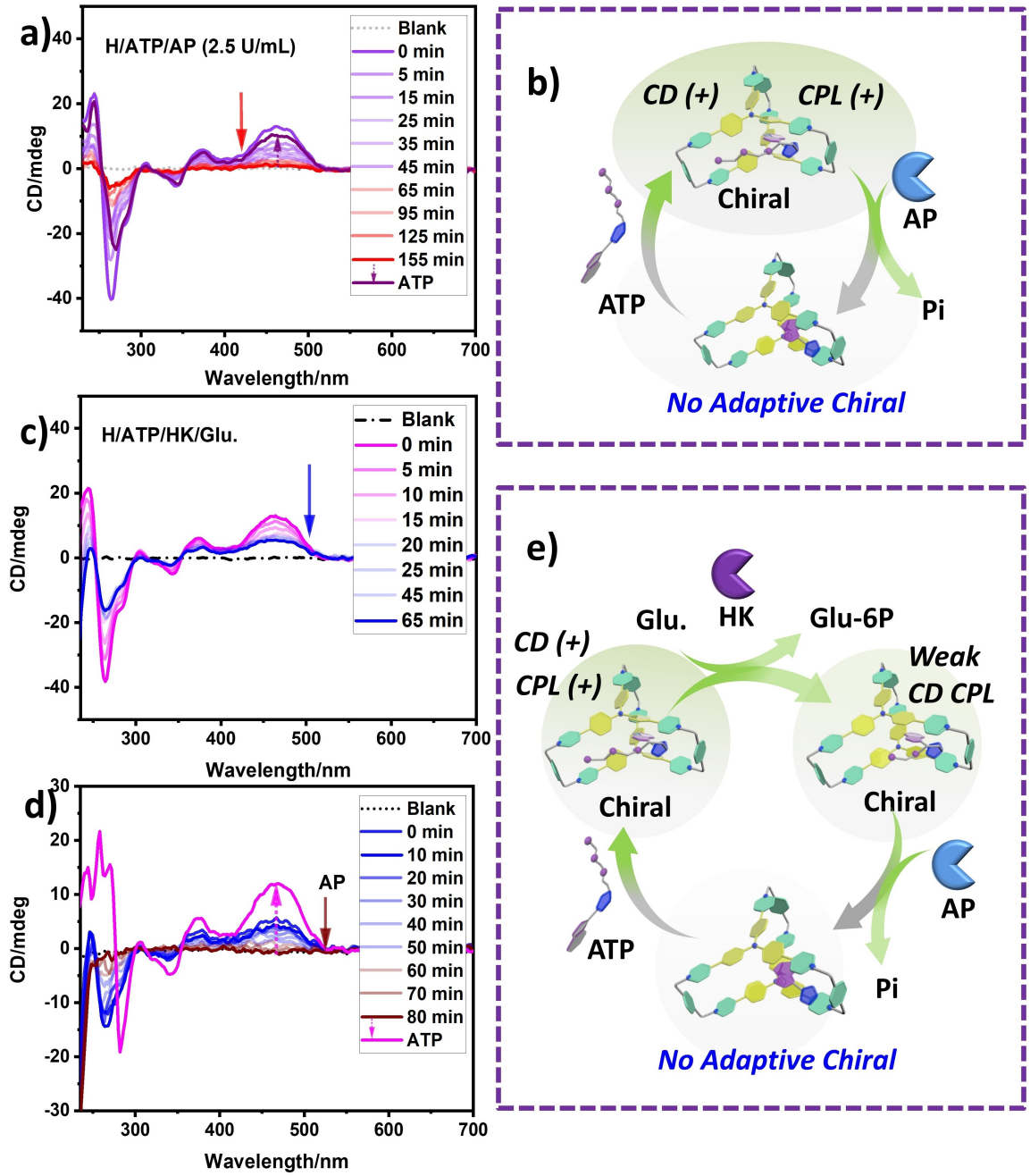

Figure 4. (a) CD spectra of H/ATP (5.0 eq.) with apyrase (AP) at 25 °C ([H] = 0.01 mM, [AP] = 2.5 U/mL). (b) Schematic illustration of ATP-driven adaptive chiral transfer supramolecule by the catalysis of AP. (c) CD spectra of H/ATP (5.0 eq.) with the addition of hexokinase (HK) and glucose (Glu.) at 25 °C ([H] = 0.01 mM, [ATP] = 0.05 mM, [Glu.] = 0.05 mM, [HK] = 7.8 U/mL). (d) CD spectra of H/ATP/HK/Glu. with AP (2.5 U/mL) at 25 °C. (e) Schematic illustration of ATP-driven stepping-regulated adaptive chiral transfer supramolecules by the catalysis of HK and AP in tandem.

diminished to 84.3 % and 10.6 %, respectively (Figures S34–35). The system's fluorescence was recovered after adding ATP (Figure S34, red arrow), exhibiting the refueled ability for luminescence. Interestingly, H/ATP gave the positive CPL signal (Figure 5e) corresponding to its fluorescence peak at 500–800 nm, and the g_{lum} was 7.1×10^{-4} (Figure 5f), showing excellent chiroptical performance. After incubation with HK, the CPL signal of H/ATP decreased, and the g_{lum} was measured as 4.0×10^{-4} (Figure 5f), further confirming that the regulation of HK could weaken the chirality transfer between host and guest. No CPL signal was observed at 575 nm in this system after the cascade catalyzed by AP (Figure 5e), indicating the adaptive chirality of the supramolecules could be dynamically regulated by different enzyme catalysis in tandem.

The above studies showed that the biofuel-ATP exhibited excellent thermal and enzyme responsiveness to regulate chiral transfer in supramolecules. Thus, ATP-driven

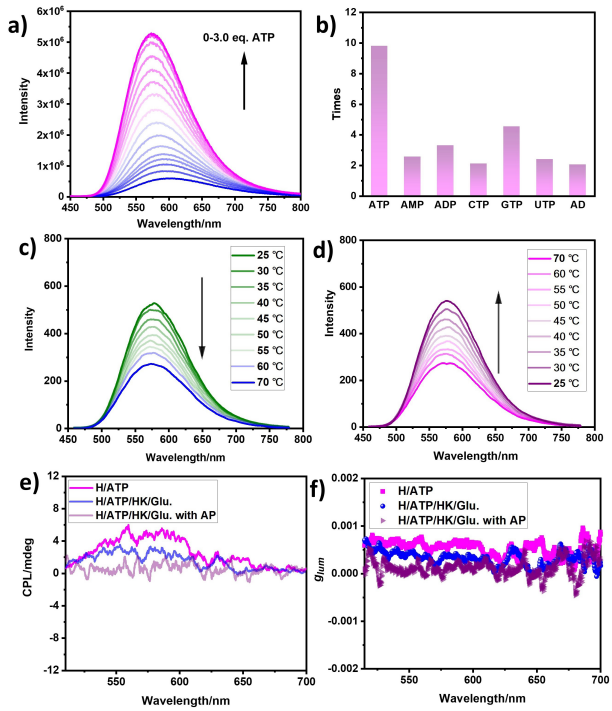

Figure 5. (a) Fluorescence spectra of H with different concentrations of ATP at 25 °C (λ_{ex} = 430 nm, [H] = 0.01 mM). (b) The fluorescence enhancement effects of H induced by nucleotides. The fluorescence spectra of H/ATP (5.0 eq.) under (c) heating and (d) cooling conditions (λ_{ex} = 430 nm, [H] = 0.01 mM). (e) The CPL spectra of H/ATP, H/ATP/HK/Glu., and H/ATP/HK/Glu. with AP at 25 °C. (f) Luminescence asymmetric factors (g_{lum}) of H/ATP, H/ATP/HK/Glu., and H/ATP/HK/Glu. with AP (λ_{ex} = 430 nm, [H] = 0.01 mM, [ATP] = 0.05 mM, [Glu.] = 0.05 mM, [HK] = 7.8 U/mL, [AP] = 2.5 U/mL).

adaptive chiral supramolecules can be applied in chiral logic gates and Morse code. The CD signal intensity of H/ATP at 465 nm was set as "output". The components of chiral supramolecules, temperature, HK, and AD were defined as "input". For output, the CD intensity at 465 nm above 7 was labeled "1" and below 7 was denoted as "0". Since the CD signal of H/ATP could be regulated by thermal and the catalysis of HK/AP, thus the temperature (45 °C) and HK/AP were set as "NOT" and "NOR" gates, respectively (Figure 6a,b). The CD intensity at 465 nm could be "locked" in the presence of H and ATP. However, the signal can be output in a "silent" model after the introduction of temperature (Figure 6a) as the "NOT" gate or HK/AP as the "NOR" gate (Figure 6b). Therefore, the obtained supramolecular chiral logic gates could output complex and reliable information. Furthermore, the supramolecular complex of H/ATP served as encryption reagents and was added to the 96-well plate, and then AP was added to corresponding wells. The Morse code signal "LJY" was observed under the illumination of 365 nm; however, after incubated 2 hours, the accurate information "TEA" was read out through the left-handed circular polarizer (Figure 6c), realizing multilevel chiral anticounterfeiting and information encryption.

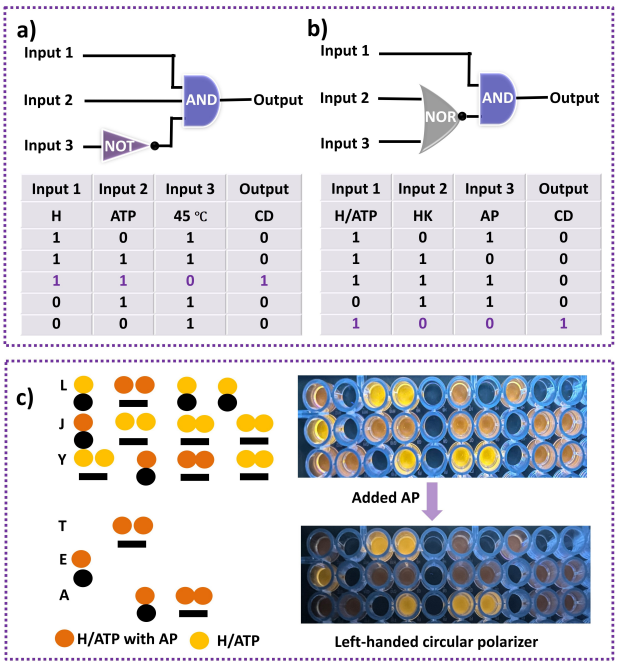

Input 1	Input 2	Input 3	Output
H	ATP	45 ℃	CD
1	0	1	0
1	1	1	0
1	1	0	1
0	1	1	0
0	0	1	0

Input 1	Input 2	Input 3	Output
H/ATP	HK	AP	CD
1	0	1	0
1	1	0	0
1	1	1	0
0	1	1	0
1	0	0	1

Figure 6. Scheme representation for (a) Temperature (45 °C) regulated INHIBIT logic gate. (b) Enzyme-regulated NOR logic gate. (c) Schematic illustration of information encryption: the Morse code under 365 nm light. The solution of H/ATP ([H] = 0.005 mM, [ATP] = 0.025 mM) and H/ATP/AP ([H] = 0.01 mM, [ATP] = 0.05 mM, [AP] = 2.5 U/mL) were added to the 96-well plate, respectively.

Conclusions

The adaptive chiral supramolecular transfer container was constructed by the hexacationic tricyclic cage as the water-soluble receptor and ATP as the biofuel, exhibiting thermal and enzyme responsiveness chirality transfer. Possessing rigid dual triphenylamine aromatic backbones, the cage could effectively encapsulate nucleotides driven by the favorable enthalpy change, giving a high binding constant of 5.37×10^5 M^{-1}. The strong binding affinity of receptors for chiral nucleotides could not only efficiently enhance the cage's luminescence performance but also activate the achiral host to give positive CD and CPL signals, realizing effective chirality transfer from the substrate to the triphenylamine cage. Notably, the adaptive chirality of supramolecules could be stepping-regulated by the catalysis of different enzymes in tandem and exhibited reversible chiral transfer under the thermal stimulus, achieving programmable regulation of multistate supramolecules with different chiroptical performance. Finally, the biofuel-driven dynamically regulated chiral supramolecular transfer containers were successfully applied in chiral logic gates and information encryption, providing a new path for chiral materials.

Acknowledgements

We thank the National Nature Science Foundation of China (22201142 and 22131008) for financial support.

Conflict of Interest

The authors declare no conflict of interest.

Data Availability Statement

The data that support the findings of this study are available from the corresponding author upon reasonable request.

Keywords: molecular recognition · supramolecular assembly · chirality transfer · stimuli-responsive · chiral anticounterfeiting

[1] E. Benchimol, J. Tessarolo, G. H. Clever, *Nat. Chem.* **2024**, *16*, 13–21.
[2] J. S. Valera, H. Arima, C. Naranjo, T. Saito, N. Suda, R. Gómez, S. Yagai, L. Sánchez, *Angew. Chem. Int. Ed.* **2022**, *134*, e202114290.
[3] S. K. Sen, R. D. Mukhopadhyay, S. Choi, I. Hwang, K. Kim, *Chem* **2023**, *9*, 624–636.
[4] M. Fellert, R. Hein, A. Ryabchun, Y. Gisbert, C. N. Stindt, B. L. Feringa, *Angew. Chem. Int. Ed.* **2024**, e202413047.
[5] J. Huang, H.-M. Ding, Y. Xu, D. Zeng, H. Zhu, D.-M. Zang, S.-S. Bao, Y.-Q. Ma, L.-M. Zheng, *Nat. Commun.* **2017**, *8*, 2131.
[6] Y. Xie, Y. Wang, W Qi, R. Huang, R. Su, Z. He, *Small* **2017**, *13*, 1700999.
[7] M. L. Ślęczkowski, M. F. J. Mabesoone, P. Ślęczkowski, A. R. A. Palmans, E. W. Meijer, *Nat. Chem.* **2021**, *13*, 200–207.
[8] T. Pal, D. Chaudhuri, *J. Am. Chem. Soc.* **2023**, *145*, 2532–2543.
[9] L. Wang, Q. Cheng, A. Hao, P. Xing, *Angew. Chem. Int. Ed.* **2023**, *62*, e202313536.
[10] Z. Li, C. J. Zeman, S. R. Valandro, J. P. O. Bantang, K. S. Schanze, *J. Am. Chem. Soc.* **2019**, *141*, 12610–12618.
[11] E. Shandilya, S. Maiti, *ACS Nano* **2023**, *17*, 5108–5120.
[12] A. Mishra, D. B. Korlepara, M. Kumar, A. Jain, N. Jonnalagadda, K. K. Bejagam, S. Balasubramanian, S. J. George, *Nat. Commun.* **2018**, *9*, 1295.
[13] S. T. Bao, S. Louie, H. Jiang, Q. Jiang, S. Sun, M. L. Steigerwald, Colin Nuckolls, Z. Jin, *J. Am. Chem. Soc.* **2024**, *146*, 51–56.
[14] A. Ramesh, T. N. Das, T. K. Maji, G. Ghosh, *Chem. Sci.* **2024**, *15*, 16355–16366.
[15] L. Zhang, H.-X. Wang, S. Li, M. Liu, *Chem. Soc. Rev*. **2020**, *49*, 9095–9120.
[16] R. G. DiNardi, S. Rasheed, S. S. Capomolla, M. H. Chak, I. A. Middleton, L. K. Macreadie, J. P. Violi, W. A. Donald, P. J. Lusby, J. E. Beves, *J. Am. Chem. Soc.* **2024**, *146*, 21196–21202.
[17] H. Guo, L.-W. Zhang, H. Zhou, W. Meng, Y.-F. Ao, D.-X. Wang, Q.-Q. Wang, *Angew. Chem. Int. Ed.* **2020**, *59*, 2623–2627.
[18] P. T. Probst, M. Mayer, V. Gupta, A. M. Steiner, Z. Zhou, G. K. Auernhammer, T. A. F. König, A. Fery, *Nat. Mater.* **2021**, *20*, 1024–1028.
[19] X. Shang, I. Song, H. Ohtsu, Y. H. Lee, T. Zhao, T. Kojima, J. H. Jung, M. Kawano, J. H. Oh, *Adv. Mater.* **2017**, *29*, 1605828.
[20] D. Zhang, H. Zheng, X. Ma, L. Su, X. Gao, Z. Tang, Y. Xu, *Adv. Opt. Mater.* **2022**, *10*, 2102015.
[21] R. A. Tromans, S. K. Samanta, A. M. Chapman, A. P. Davis, *Chem. Sci.* **2020**, *11*, 3223–3227.
[22] L. Gu, W. Ye, X. Liang, A. Lv, H. Ma, M. Singh, W. Jia, Z. Shen, Y. Guo, Y. Gao, H. Chen, D. Wang, Y. Wu, J. Liu, H. Wang, Y.-X. Zheng, Z. An, W. Huang, Y. Zhao, *J. Am. Chem. Soc.* **2021**, *143*, 18527–18535.
[23] T. Ogoshi, T. Akutsu, D. Yamafuji, T. Aoki, T. Yamagishi, *Angew. Chem. Int. Ed.* **2013**, *52*, 8111–8115.
[24] W. Zhi, Z. Pu, C. Ma, K. Liu, X. Wang, J. Huang, Y. Xiao, Y. Yan, *ACS Nano* **2021**, *15*, 19621–19628.
[25] H. Zhu, Q. Li, B. Shi, H. Xing, Y. Sun, S. Lu, L. Shangguan, X. Li, F. Huang, P. J. Stang, *J. Am. Chem. Soc.* **2020**, *142*, 17340–17345.
[26] J. Yu, J. Niu, X. Xu, Y. Liu, *Adv. Sci.* **2024**, *11*, 2408107.
[27] S. Erbas-Cakmak, D. A. Leigh, C. T. McTernan, A. L. Nussbaumer, *Chem. Rev.* **2015**, *115*, 10081–10206.
[28] J.-L. Bégin, A. Jain, A. Parks, F. Hufnagel, P. Corkum, E. Karimi, T. Brabec, R. Bhardwaj, *Nat. Photonics* **2023**, *17*, 82–88.
[29] G. Preda, S. Jung, G. Pescitelli, L. Cupellini, D. Armspach, D. Pasini, *Chem. Eur. J.* **2023**, *29*, e202302376.
[30] J.-H. Huang, Y.-J. Liu, Y. Si, Y. Cui, X.-Y. Dong, S.-Q. Zang, *J. Am. Chem. Soc.* **2024**, *146*, 16729–16736.
[31] C. Tu, W. Wu, W. Liang, D. Zhang, W. Xu, S. Wan, W. Lu, C. Yang, *Angew. Chem. Int. Ed.* **2022**, *61*, e202203541.
[32] S. Fa, T. Tomita, K. Wada, K. Yasuhara, S. Ohtani, K. Kato, M. Gon, K. Tanaka, T. Kakuta, T.-A. Yamagishi, T. Ogoshi, *Chem. Sci.* **2022**, *13*, 5846–5853.
[33] X.-Y. Lou, K. Zhang, Y. Bai, S. Zhang, Y. Li, Y.-W. Yang, *Angew. Chem. Int. Ed.* **2024**, e202414611.
[34] E. Lee, H. Ju, I.-H. Park, J. H. Jung, M. Ikeda, S. Kuwahara, Y. Habata, S. S. Lee, *J. Am. Chem. Soc.* **2018**, *140*, 9669–9677.
[35] M. Kazem-Rostami, A. Orte, A. M. Ortuño, A. H. G. David, I. Roy, D. Miguel, A. Garci, C. M. Cruz, C. L. Stern, J. M. Cuerva, J. F. Stoddart, *J. Am. Chem. Soc.* **2022**, *144*, 9380–9389.
[36] W.-J. Li, Q. Gu, X.-Q. Wang, D.-Y. Zhang, Y.-T. Wang, X. He, W. Wang, H.-B. Yang, *Angew. Chem. Int. Ed.* **2021**, *60*, 9507–9515.
[37] T. Zhao, J. Han, P. Duan, M. Liu, *Acc. Chem. Res.* **2020**, *53*, 1279–1292.
[38] C. Zhao, Y. Wang, Y. Jiang, N. Wu, H. Wang, T. Li, G. Ouyang, M. Liu, *Adv. Mater.* **2024**, *36*, 2403329.
[39] L. Hu, X. Zhu, C. Yang, M. Liu, *Angew. Chem. Int. Ed.* **2022**, *61*, e202114759.
[40] A. M. Agafontsev, A. Ravi, T. A. Shumilova, A. S. Oshchepkov, E. A. Kataev, *Chem. Eur. J.* **2019**, *25*, 2684–2694.
[41] U. Tamima, S. Sarkar, M. R. Islam, A. Shil, K. H. Kim, Y. J. Reo, Y. W. Jun, H. Banna, S. Lee, K. H. Ahn, *Angew. Chem. Int. Ed.* **2023**, *62*, e202300580.
[42] J. Kong, Z. Liu, D. Cai, Y. Fan, P. Zhao, X. Liu, P. Pu, L. Song, C. He, *Sens. Actuators B* **2018**, *256*, 913–920.
[43] B. S. Morozov, F. Gargiulo, S. Ghule, D. J. Lee, F. Hampel, H. M. Kim, E. A. Kataev, *J. Am. Chem. Soc.* **2024**, *146*, 7105–7115.
[44] S. Maji, J. Samanta, R. Natarajan, *Chem. Eur. J.* **2024**, *30*, e202303596.
[45] L. Cheng, K. Liu, Y. Duan, H. Duan, Y. Li, M. Gao, L. Cao, *CCS Chem.* **2021**, *3*, 2749–2763.
[46] L. Zhao, L. Cheng, Y. Yang, P. Wang, P. Tian, T. Yang, H. Nian, L. Cao, *Angew. Chem. Int. Ed.* **2024**, *63*, e202405150.
[47] J. González-García, S. Tomić, A. Lopera, L. Guijarro, I. Piantanida, E. García-España, *Org. Biomol. Chem.* **2015**, *13*, 1732–1740.
[48] H. Nian, L. Cheng, L. Wang, H. Zhang, P. Wang, Y. Li, L. Cao, *Angew. Chem. Int. Ed.* **2021**, *60*, 15354–15358.

[49] J. Yu, J. Niu, J. Yue, L.-H. Wang, Y. Liu, *ACS Nano* **2023**, *17*, 19349–19358.
[50] S. Mommer, K. Sokołowski, M. Olesińska, Z. Huang, O. A. Scherman, *Chem. Sci.* **2022**,*13*, 8791–8796.
[51] T.-H. Shi, Y. Nagata, S. Akine, S. Ohtani, K. Kato, T. Ogoshi, *J. Am. Chem. Soc.* **2022**, *144*, 23677–23684.
[52] J. J. Tarrío, R. Rodríguez, J. Crassous, E. Quiñoá, F. Freire, *Angew. Chem. Int. Ed.* **2023**, *62*, e202307059.
[53] R. N. Dsouza, A. Hennig, W. M. Nau, *Chem. Eur. J.* **2012**, *18*, 3444–3459.

Manuscript received: October 1, 2024
Accepted manuscript online: November 8, 2024
Version of record online: ■■, ■■

Communication

Chirality Transfer

J. Yu, H. Yu, Y. Qiu, H.-Y. Zhang, X. Xu, Y. Liu* e202418938

Biofuel-Driven Stepping Chiral Supramolecular Transfer Container

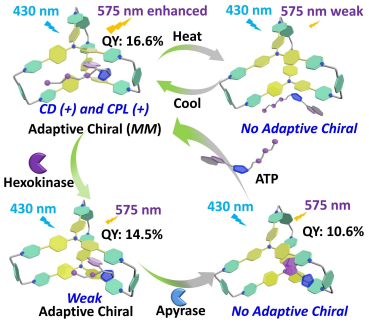

The biofuel-mediated adaptive chiral luminescent supramolecular transfer container exhibited reversible thermal responsiveness and stepping-regulated chirality transfer by the catalysis of enzymes in tandem, as well as recovered chirality after refueled, achieving programmable regulation of multistate supramolecular chiroptical performance, which was successfully applied in logic gates and information encryption.